2010

Multiple Spacecraft Assembly Maneuvers by Differential Drag and Low Thrust Engines

Bevilacqua, R.; Hall, J.S.; Romano, M.

Bevilacqua, R.,Hall, J., S., Romano, M., Multiple Spacecraft Assembly Maneuvers by Differential Drag and Low Thrust Engines, Celestial Mechanics and Dynamical Astronomy (2010) 106:6988, DOI 10.1007/s10569-009-9240-3.
http://hdl.handle.net/10945/38451

Celest Mech Dyn Astr (2010) 106:69–88
DOI 10.1007/s10569-009-9240-3

ORIGINAL ARTICLE

Multiple spacecraft rendezvous maneuvers by differential drag and low thrust engines

Riccardo Bevilacqua · Jason S. Hall · Marcello Romano

Received: 31 October 2008 / Revised: 5 October 2009 / Accepted: 19 October 2009 /
Published online: 27 November 2009

Abstract A novel two-phase hybrid controller is proposed to optimize propellant consumption during multiple spacecraft rendezvous maneuvers in Low Earth Orbit. This controller exploits generated differentials in aerodynamic drag on each involved chaser spacecraft to effect a propellant-free trajectory near to the target spacecraft during the first phase of the maneuver, and then uses a fuel optimal control strategy via continuous low-thrust engines to effect a precision dock during the second phase. In particular, by varying the imparted aerodynamic drag force on each of the chaser spacecraft, relative differential accelerations are generated between each chaser and the target spacecraft along two of the three translational degrees of freedom. In order to generate this required differential, each chaser spacecraft is assumed to include a system of rotating flat panels. Additionally, each chaser spacecraft is assumed to have continuous low-thrust capability along the three translational degrees of freedom and full-axis attitude control. Sample simulations are presented to support the validity and robustness of the proposed hybrid controller to variations in the atmospheric density along with different spacecraft masses and ballistic coefficients. Furthermore, the proposed hybrid controller is validated against a complete nonlinear orbital model to include relative navigation errors typical of carrier-phase differential GPS (CDGPS). Limitations of the proposed controller appear relative to the target spacecraft's orbit eccentricity and a general characterization of the atmospheric density. Bounds on these variables are included

R. Bevilacqua (✉)
Department of Mechanical and Astronautical Engineering, Naval Postgraduate School, Code MAE/RB, 700 Dyer Rd., Monterey, CA 93943, USA
e-mail: rbevilac@nps.edu

J. S. Hall
Department of Mechanical and Astronautical Engineering, Naval Postgraduate School, Code AA/JH, 699 Dyer Rd., Monterey, CA 93943, USA
e-mail: jasonshall@ymail.com

M. Romano
Department of Mechanical and Astronautical Engineering, Naval Postgraduate School, Code MAE/MR, 700 Dyer Rd., Monterey, CA 93943, USA
e-mail: mromano@nps.edu

to provide a framework within which the proposed hybrid controller can effect an extremely low propellant rendezvous of multiple chaser spacecraft to a desired target spacecraft.

Keywords Multiple spacecraft rendezvous · Differential drag · Optimal control · Autonomous rendezvous

List of symbols

a_T	Target spacecraft semi-major axis
c	Coefficient in Schweighart–Sedwick equations
C_{D_T}	Target spacecraft drag coefficient
$C_{D_{C_i}}$	ith chaser spacecraft drag coefficient
${}^{O}\mathbf{r}_{C_i}$	Relative position vector of the ith chaser spacecraft in LVLH orbital frame
${}^{O}\mathbf{v}_{C_i}$	Relative velocity vector of the ith chaser spacecraft in LVLH orbital frame
ΔBC	Ballistic coefficient differential
$\Delta BC_{C_i,\max}$	ith chaser spacecraft maximum ballistic coefficient differential which corresponds to the maximum relative acceleration differential
$\Delta BC_{C_i,\min}$	ith chaser spacecraft minimum ballistic coefficient differential which corresponds to the minimum relative acceleration differential
Δt	Time interval used in fuel-optimal control solution
Δt_{opt}	Waiting time between re-solving the fuel-optimal low-thrust control sequence
Δt^*	Switching time for the differential-drag controlled rendezvous phases
ΔV	Metric for fuel consumption expressed in terms of total velocity variation
ECI	Earth centered inertial coordinate frame
e_0	Time-varying eccentricity of the Harmonic Oscillator Motion before Rendezvous
e_T	Target spacecraft orbit eccentricity
$\mathbf{\Phi}(t)$	State transition matrix for relative motion equations
ϕ	Phase of forcing term in out-of-plane motion in Schweighart–Sedwick equations
$h(t_0)$	Target spacecraft initial altitude above the Earth surface
I	Metric for fuel consumption expressed in total impulse
I_{nxn}	nxn Identity Matrix
ISS	International Space Station
i_T	Target spacecraft orbit inclination
J_2	Second-order harmonic of Earth gravitational potential field (Earth flattening) [108263×10^{-8}, cf. Vallado 2004]
J	Cost function
LVLH	Local Vertical Local Horizontal
l	Coefficient in Schweighart–Sedwick equations (out-of-plane motion)
$\boldsymbol{\lambda}_r$	Position co-state vector
$\boldsymbol{\lambda}_V$	Velocity co-state vector
m_T	Target spacecraft mass
m_{C_i}	ith chaser spacecraft mass
ν_T	Target spacecraft orbit initial anomaly
ω	Target spacecraft orbital angular rate
ω_T	Target spacecraft orbit argument of perigee
Ω_T	Target spacecraft orbit right ascension of ascending node (RAAN)

$\mathbf{\Psi}(t)$	Convolution integral matrix for relative motion equations due to optimal unbounded control
q	Coefficient in Schweighart–Sedwick equations (out-of-plane motion)
$R_\oplus$	Earth mean radius (6378.1363 km, cf. Vallado 2004)
r_T	Target spacecraft reference orbit radius
ρ	Atmospheric density
S_T	Target spacecraft cross-wind section area
$S_{C_i,\min}$	ith chaser spacecraft minimum cross-wind section area
$S_{C_i,\max}$	ith chaser spacecraft maximum cross-wind section area
$S_{C_i 0}$	ith chaser spacecraft cross-wind section area to achieve zero ballistic coefficient differential
S_P	Single drag plate cross-wind section area
σ_{pos}	Variance of the relative position errors
σ_{vel}	Variance of the relative velocity errors
t	Time
$\mathbf{u}$	Control vector
u_x, u_y, u_z	Control variables expressed as relative accelerations in the LVLH orbital frame
V_r	Spacecraft velocity vector magnitude with respect to the Earth's atmosphere
$\mathbf{x}$	Spacecraft relative state vector
$\mathbf{z}$	Transformed spacecraft relative state vector
$z_{1,\text{tol}}, z_{2,\text{tol}}$	Tolerances in reaching a stable orbit
t_0	Initial time
t_f	Final time

1 Introduction

The possibility of controlling spacecraft relative motion by exploiting the Earth's atmosphere has been studied for several years (Leonard 1986; Leonard et al. 1989; Humi and Carter 2001; Palmerini et al. 2005) and is still an open topic of research (Kumar and Ng 2008; Bevilacqua and Romano 2008). Growing interest in exploiting differential aerodynamic drag for real-world small spacecraft design is evidenced in the current JC2Sat (De Ruiter et al. 2008) being developed by the Canadian Space Agency and the Japanese Space Agency, and the InKlajn-1 being developed at the Israel Aerospace Industries (Winetraub and Tamir 2009). When atmospheric differential drag is used for spacecraft rendezvous, an under-actuated controllable system exists in two of the three translational degrees of freedom, namely the target spacecraft's orbital plane (Campbell 2003; Kumar et al. 2007; Starin et al. 2001). With respect to the full relative motion system to include the out-of-plane motion, several propellant optimized control methods have been proposed that involve long duration low-thrust maneuvers (Bevilacqua and Romano 2007; Guelman and Aleshin 2001; Humi and Carter 2001).

In this work, a novel two-phase hybrid approach is proposed that is based on a combination of differential aerodynamic drag and continuous low-thrust optimal control to affect quasi propellant-free rendezvous maneuvers for an arbitrary number of spacecraft. Both phases are implemented in feedback with respect to the spacecraft relative states to account for unmodeled dynamics and disturbances. The first phase, which involves the approach of the chaser spacecraft from a far away initial condition to an orbit near to the target spacecraft, is accomplished propellant-free by differential aerodynamic drag utilizing a system of paddles

on the chaser spacecraft. During the second phase, low-thrust engines are used to complete the precise rendezvous using a fuel optimal control strategy.

The main contributions of this paper to the state of the art for multiple spacecraft rendezvous control can be summarized as follows:

1. Important analytical developments on previously obtained results on differential drag precise rendezvous (Bevilacqua and Romano 2008).
2. Design of a differential drag-based feedback controller that requires no coasting phases and thus can be implemented stand-alone on each chaser spacecraft. This new approach provides the following key benefits
   a. No waiting time is needed among different spacecraft to maneuver closer to the target. This drastically reduces the maneuver overall required time;
   b. The target does not modify its cross-wind section area, i.e. it does not increase its natural orbit decay. This is in contrast to previous work in which the control of the system of multiple spacecraft depended on a maneuvering target spacecraft with similar drag plates (Bevilacqua and Romano 2008).
3. Introduction of a two-phase hybrid technique to obtain low propellant spacecraft rendezvous maneuvers by which a seamless integration between an existing rendezvous optimal controller (Guelman and Aleshin 2001) and the proposed differential drag-based controller is demonstrated.
4. Test of the proposed linear models-based feedback techniques against a complete nonlinear model that includes realistic relative navigation errors and uncertainties on the atmospheric density.
5. Capability of maneuvering spacecraft with different masses and ballistic coefficients.
6. Robustness against poor characterization of the atmospheric density whereby the proposed hybrid controller requires only an initial estimation of the atmospheric density.
7. Delineation of boundaries for the target's orbit eccentricity and for the initial guess on the atmospheric density in order to successfully utilize the proposed hybrid controller.

It is worth mentioning that the use of drag plates for a single rendezvous between a target and a chaser would probably add more onboard weight than using fuel alone. Nevertheless, the proposed approach is envisioned for multiple rendezvous maneuvers, formation-keeping, etc., where the trade-off between fuel saving and increased weight due to the installation of drag plates may be very advantageous.

The paper is organized as follows. Section 2 introduces the dynamics model and control logic used for the differential drag controller design. Section 3 illustrates the optimal low-thrust approach for the final phase of the rendezvous maneuver. Section 4 describes the validation of the drag controller and the optimal low-thrust controller with a nonlinear orbital propagator and a realistic spacecraft model. Section 5 is dedicated to numerical simulations. For the presented simulations the target spacecraft is set at an orbit similar to that of the International Space Station (ISS). The eccentricity is increased with respect to that of the ISS, in order to test the approach capability of dealing with eccentric orbits. Furthermore, a subsection of Sect. 5 lists the main boundaries for using the hybrid control here presented. Section 6 concludes the paper.

2 Dynamics model including J_2 and control via differential drag

In this section the analytical developments for the dynamics and control of the spacecraft relative motion via differential drag are presented. The differential drag control logic is used in the first phase of the multi-spacecraft rendezvous maneuvers. The relative dynamics between two generic spacecraft, considering the averaged effect of the J_2 perturbation over one orbit, projected in the LVLH coordinate system with respect to the target spacecraft, is represented by the Schweighart–Sedwick equations (Schweighart et al. 2002)

$$\dot{\mathbf{x}} = \begin{bmatrix} 0_{3\times3} & I_{3\times3} \\ A_1 & A_2 \end{bmatrix} \mathbf{x} + \begin{bmatrix} 0_{3\times3} \\ I_{3\times3} \end{bmatrix} \mathbf{u} \tag{1}$$

with state vector $\mathbf{x}(t) \in \mathbb{R}^6$, $\forall \mathbf{x}^T = [x, y, z, \dot{x}, \dot{y}, \dot{z}] = \left[{}^O\mathbf{r}_{C_i}, {}^O\mathbf{v}_{C_i}\right]$, control vector $\mathbf{u}(t) \in \mathbb{R}^3$, $\forall \mathbf{u}^T = \left[u_x, u_y, u_z + 2lq\cos(qt + \phi)\right]$ and

$$A_1 = \begin{bmatrix} 5c^2\omega^2 - 2\omega^2 & 0 & 0 \\ 0 & 0 & 0 \\ 0 & 0 & -q^2 \end{bmatrix}, \quad A_2 = \begin{bmatrix} 0 & 2\omega c & 0 \\ -2\omega c & 0 & 0 \\ 0 & 0 & 0 \end{bmatrix} \tag{2}$$

The dynamics of Eq. 1 assumes:

1. circular reference orbit;
2. close separations between spacecraft (in comparison to their orbital radius);
3. the only acting forces are 2-body, J_2 gravity and control.

The Schweighart–Sedwick LVLH coordinate system is defined as follows: the x axis is collinear with the position vector of the target spacecraft, the y axis is in the direction of the velocity vector along the orbital track and the z axis is normal to the orbital plane completing a right-hand Cartesian coordinate system. l, q and ϕ are coefficients as defined in Schweighart et al. (2002), ω represents the current angular rate of the LVLH frame and c is defined as

$$c = \sqrt{1 + \frac{3J_2R_\oplus^2}{8r_T^2}\left[1 + 3\cos(2i_T)\right]} \tag{3}$$

with J_2 representing the second order harmonic of Earth's gravitational potential field, $R_\oplus$ the Earth's mean radius, r_T the magnitude of the position vector of the target spacecraft in the Earth Centered Inertial (ECI) coordinate frame, and i_T the inclination of the target spacecraft.

Furthermore, the control vector $\mathbf{u}$ indicates the components of the relative acceleration between the two spacecraft. When only differential aerodynamic drag is considered, the control vector becomes

$$\mathbf{u}^T = \begin{bmatrix} 0 & -\frac{\rho\Delta BC}{2}V_r^2 & 0 \end{bmatrix} \tag{4}$$

where ρ is the atmospheric density, V_r is the magnitude of the spacecraft velocity vector with respect to Earth's atmosphere, and ΔBC is the ballistic coefficient differential given by

$$\Delta BC = BC_{C_i} - BC_T = \frac{m_T C_{D_{C_i}} S_{C_i} - m_{C_i} C_{D_T} S_T}{m_T m_{C_i}} \tag{5}$$

with m_T, m_{C_i} representing the mass of the target and ith chaser spacecraft respectively, $C_{D_T}, C_{D_{C_i}}$ representing the coefficient of drag of the target and ith chaser spacecraft respectively, and S_T, S_{C_i} representing the wind-cross section area of the target and ith chaser spacecraft respectively. The ballistic coefficient differential accounts for different masses,

drag coefficients and wind-cross section areas between the chaser spacecraft and target spacecraft. The atmospheric density and the magnitude of the spacecraft velocity vector are in first approximation retained constant between them. The possibility of non homogenous spacecraft was not taken into account by the original approach described in Bevilacqua and Romano (2008) and presents one of the key benefits to the presented approach.

By disregarding the out-of-plane motion, which cannot be controlled by considering only differential aerodynamic drag, the relative dynamics of two generic spacecraft given by Eq. 1 become linear in

$$\dot{\mathbf{x}} = \begin{bmatrix} 0_{2x2} & I_{2x2} \\ A_1 & A_2 \end{bmatrix} \mathbf{x} + \begin{bmatrix} 0_{2x2} \\ I_{2x2} \end{bmatrix} \mathbf{u} \tag{6}$$

with state vector $\mathbf{x}(t) \in \mathbb{R}^6, \forall \mathbf{x}^T = [x, y, \dot{x}, \dot{y}]$, control vector $\mathbf{u}(t) \in \mathbb{R}^3, \forall \mathbf{u}^T = \begin{bmatrix} u_x, u_y \end{bmatrix}$ and

$$A_1 = \begin{bmatrix} 5c^2\omega^2 - 2\omega^2 & 0 \\ 0 & 0 \end{bmatrix}, \quad A_2 = \begin{bmatrix} 0 & 2\omega c \\ -2\omega c & 0 \end{bmatrix} \tag{7}$$

Equation 6 can further be decomposed into a double integrator and a harmonic oscillator via the following state vector transformation

$$\mathbf{z} = \begin{bmatrix} 0 & 1 & -a/d^2 & 0 \\ -ab/d^2 & 0 & 0 & -b/d^2 \\ 0 & 0 & a^2/(2d^3) & 0 \\ a^2b/(2d^3) & 0 & 0 & a^3/(2d^3) \end{bmatrix} \mathbf{x} \tag{8}$$

where $\mathbf{z}(t) \in \mathbb{R}^4, \forall \mathbf{z}^T = [z_1, z_2, z_3, z_4]$ and $a = 2\omega c, b = \left(5c^2 - 2\right)\omega^2, d = \sqrt{a^2 - b}$.

The dynamics in the new state vector (see also Bevilacqua et al. 2009; Bevilacqua and Romano 2008) have the following closed form solution for constant control acceleration u_y with $u_x = 0$

$$\begin{aligned} z_1 &= z_{1_0} + t z_{2_0} - \tfrac{bt^2}{2d^2} u_y \\ z_2 &= z_{2_0} - \tfrac{bt}{d^2} u_y \\ z_3 &= \cos(dt)\, z_{3_0} + \tfrac{\sin(dt)}{d} z_{4_0} + \tfrac{a^3[1-\cos(dt)]}{2d^5} u_y \\ z_4 &= -d \sin(dt)\, z_{3_0} + \cos(dt)\, z_{4_0} + \tfrac{a^3 \sin(dt)}{2d^4} u_y \end{aligned} \tag{9}$$

The two aspects of the relative motion dynamics can be represented in two different phase planes. Figure 1a represents the double integrator motion, Fig. 1b the harmonic oscillator part.

When using differential aerodynamic drag for control of the linear dynamics given by Eq. 6, a system of drag plates are imagined to be mounted on each spacecraft so that direction of relative acceleration can be controlled (see Eq. 4 given Eq. 5: ΔBC can be either zero, negative or positive). Furthermore, some assumptions are made in order to exploit the analytical solution in Eq. 9 for designing the control logic (Bevilacqua and Romano 2008). These are only used for the analytical developments of the drag control logic and include

1. The angle of attack of the drag plates of each spacecraft can be instantaneously either 0 or 90°, thus generating a minimum (Fig. 2, CASE 1), zero (Fig. 2, CASE 2) or a maximum (Fig. 2, CASE 3) relative drag acceleration. This assumption is removed in simulations by providing a linear rotation. Furthermore, the drag plates are considered to rotate in couples, as depicted in Fig. 2, CASE 2.

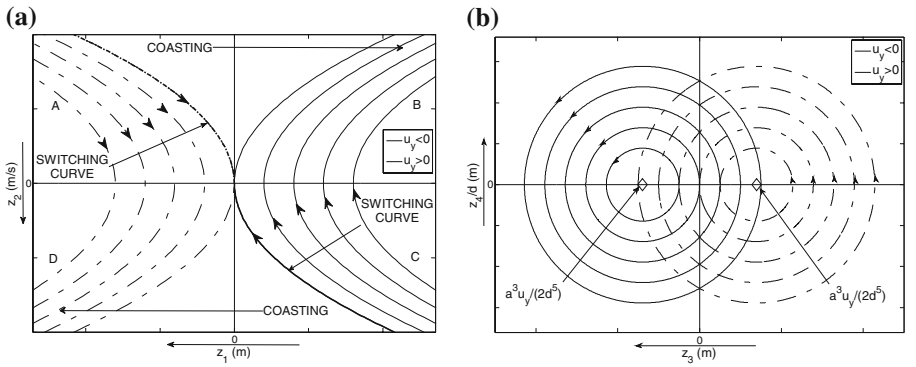

Fig. 1 Qualitative shape of the curves representing the relative motion of a chaser spacecraft with respect to the target in the z-phase plane. **a** Curves in $z_1 z_2$, **b** curves in $z_3(z_4/d)$ (modified from Bevilacqua and Romano 2008)

2. Attitude dynamics are not considered. Attitude is assumed to be stabilized in the LVLH coordinate system.
3. The atmospheric density ρ is constant for all of the spacecraft and equal to that of the target's altitude at the initial time $(h(t_0))$. This assumption is removed in simulations to include a modeled atmospheric density with a bias offset.
4. The problem is confined to the xy plane with the final condition for each chaser being the equilibrium point where $\mathbf{x} = \mathbf{0}$. The dynamics along the z-axis, which is oscillatory and independent from the dynamics in the xy plane, is left uncontrolled during the differential aerodynamic drag phase.
5. The target orbital rate ω is constant during the maneuver. This assumption is removed in simulations.

The drag plates concept illustrated in Fig. 2 represents an evolution and significant enhancement of the ideas previously introduced by Bevilacqua and Romano (2008). In particular, with respect to the herein proposed two-phase hybrid controller, the target spacecraft's ballistic coefficient is taken to be constant while each individual chaser spacecraft is capable of changing its ballistic coefficient such that a negative, zero or positive control is generated with respect to the target. By this new assumption, the algorithm presented in Bevilacqua and Romano (2008) is simplified in that any mutual constraints among the control signs of the chasers are removed.

The control during the differential drag phase of the hybrid controller involves closed loop orbit stabilization of each chaser spacecraft with respect to the target equivalent to what is presented in Bevilacqua and Romano (2008) when considering only one chaser spacecraft. This occurs in the ideal case when $z_1 = z_2 = 0$ but can be readily modified to accept a near-stable orbit by considering a tolerance on each phase plane parameter. The stable motion can be either a leader-follower configuration or a closed relative orbit described by the chaser around the target (For more details, see Bevilacqua and Romano 2008; Leonard 1986; Leonard et al. 1989). After stabilization, precise rendezvous in the orbital plane is attempted by an analytically determined switching control sequence as shown in Fig. 3. In this open loop switching control sequence, a series of four switching times $(n\Delta t^*, n = 1, 2, 3, 4)$ are calculated that include a waiting phase with $u_y = 0$, a positive or negative generated u_y, two sign changes in u_y and then a final $u_y = 0$. The goal of this sequence is to affect a smooth rendezvous trajectory with the target spacecraft. In fact, in the ideal case where the target and chaser have

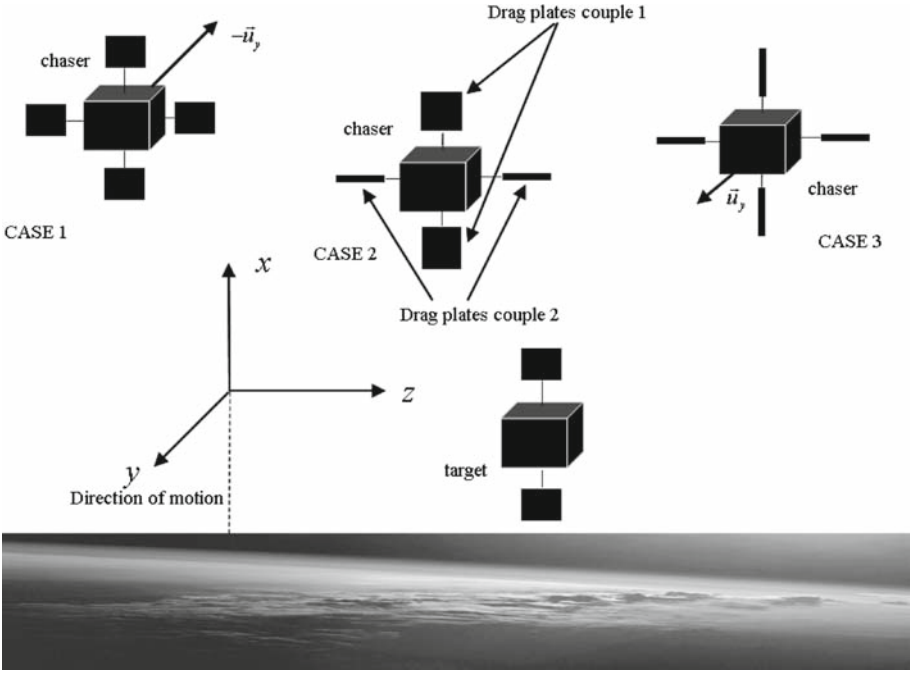

Fig. 2 Illustration of the proposed drag plates concept

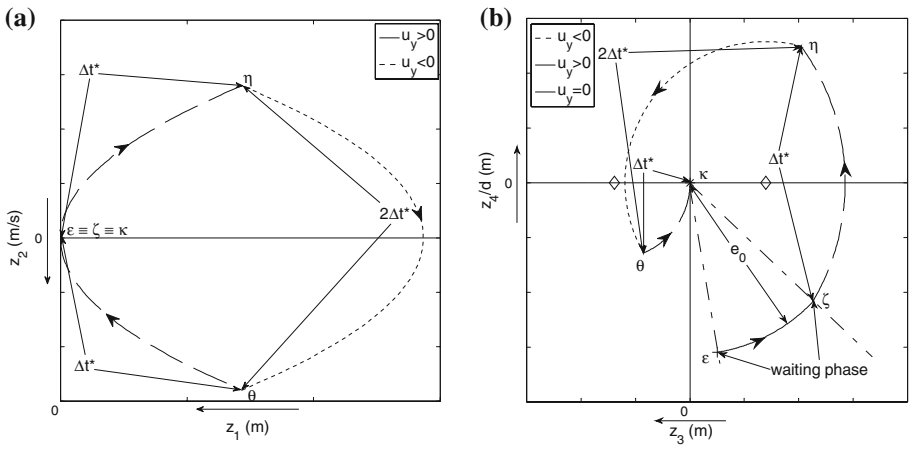

Fig. 3 Qualitative examples of rendezvous maneuver in the phase planes. **b** The *plus symbol* indicates the initial state, and the *star symbol* indicates the final condition. **a** Rendezvous trajectory in the $z_1 z_2$ plane; **b** rendezvous trajectory in the $z_3(z_4/d)$ plane (modified from Bevilacqua and Romano 2008)

identical characteristics, the atmospheric density is precisely modeled, the target spacecraft is in a perfectly circular orbit and there is no out-of-plane motion, this control sequence will affect a precise rendezvous of the chaser with the target.

In particular, the value of Δt^* used in the control sequence in Fig. 3 is represented by

$$\Delta t^* = \frac{1}{d}\cos^{-1}\left[1/2\left(1+\sqrt{h}-\sqrt{3-h-2/\sqrt{h}}\right)\right] \tag{10}$$

where

$$\begin{aligned} h &= 1+\sqrt[3]{f}/6g - e_0^2/g\sqrt[3]{f} \\ f &= -54ge_0^2 + 6\sqrt{3}e_0^2\sqrt{2e_0^2+27g^2} \\ g &= -\frac{\sqrt{2}}{2}\frac{a^3|u_y|}{d^5}i \end{aligned} \tag{11}$$

The following represent important new developments with respect to the selection of Δt^* and allow for specific implementation in a real-world environment with biased atmospheric density and other perturbations. In order for the argument of the inverse cosine in Eq. 10 to not exceed the unit value, the following condition must be satisfied

$$e_0 = \sqrt{z_3^2 + (z_4/d)^2} < \frac{13}{5}\frac{a^3\,|u_y|}{d^5} \tag{12}$$

with z_3 and z_4/d corresponding to the appropriate transformed coordinates following Eq. 8 at the beginning of the rendezvous trajectory starting from the nearly stable orbit.

If this condition is not satisfied at the beginning of the switching control sequence, the e_0 is adjusted to

$$e_0 = e_0 - 0.99\left(\frac{13}{5}\frac{a^3\,|u_y|}{d^5}\right) \tag{13}$$

and substituted into Eq. 11 to find the switching times Δt^* given by Eq. 10. Upon executing this control sequence, the chaser spacecraft will be at a new, smaller, stable orbit from which Eq. 13 can be re-applied, if necessary, until the condition of Eq. 12 is satisfied.

3 Optimal low-thrust close proximity maneuvers

Using the differential drag control described in the previous section against a true nonlinear model complete with varying atmospheric density, errors arise in matching the final desired state vectors of the chaser spacecraft. Furthermore, the differential drag control presented does not deal with the out of plane motion. For these reasons, a fuel optimal controller based on continuous low-thrust engines is proposed for the final precision rendezvous maneuver. This controller builds upon the results of Guelman and Aleshin (2001).

If the chaser spacecraft are in the vicinity of the target, the linear dynamics expressed in Eq. 1 given Eq. 2 can be used with no major issues caused by the linear approximation and by neglecting un-modeled disturbances. However, in order to significantly reduce the effects of the nonlinearity and un-modeled disturbances, the fuel-optimal solution of Guelman and Aleshin (2001), modified to include the Schweighart–Sedwick equations of Eq. 1 as a substitute for the Hill–Clohessy–Wiltshire (Clohessy–Wiltshire 1960) equations of motion, is implemented in such a way that it can be repetitively computed at fixed time steps. This is accomplished in a feedback fashion with respect to the spacecraft relative state vector.

By assuming continuous thrust capability in all three translational degrees of freedom, the fuel optimal control problem of Guelman and Aleshin (2001) can be applied to the

relative motion equations of Eq. 1. Given the initial and final conditions for the state vector $\mathbf{x}^T = [x, y, z, \dot{x}, \dot{y}, \dot{z}] = \left[{}^{O}\mathbf{r}_{C_i}, {}^{O}\mathbf{v}_{C_i}\right]$ and a time interval to perform the maneuver $\Delta t = t_f - t_0$, the goal of the fuel optimal controller is to minimize the cost function

$$J = \frac{1}{2}\int_{t_1}^{t_2} \mathbf{u}^T \mathbf{u} dt \tag{14}$$

subject to the constraints

$$|u_k| \leq F_{\max}/m_{C_i}, \qquad k = x, y, z, \quad i = 1, 2, \ldots, n \tag{15}$$

With respect to the proposed two-phase hybrid controller, the initial state vector of the generic chaser spacecraft is taken to be its state at the end of phase one, the differential drag control phase, and the final desired state vector is the 6-by-1 null vector.

The Hamiltonian of the problem is

$$H = \frac{1}{2}\mathbf{u}^T\mathbf{u} + \boldsymbol{\lambda}_r^T \mathbf{r} + \boldsymbol{\lambda}_v^T (A_1 \mathbf{r} + A_2 \mathbf{v} + \mathbf{u}) \tag{16}$$

where $\boldsymbol{\lambda}_r(t) \in \mathbb{R}^{3x1}, \forall \boldsymbol{\lambda}_r^T = [\lambda_1, \lambda_2, \lambda_3]$ and $\boldsymbol{\lambda}_v(t) \in \mathbb{R}^{3\times 1}, \forall \boldsymbol{\lambda}_v^T = [\lambda_4, \lambda_5, \lambda_6]$ are the co-state vectors. By applying the minimum principle (Pontryagin et al. 1969) and considering the constraints in Eq. 15, the optimal control law is given by

$$\begin{aligned} u_k &= -\lambda_{V_k} \quad \text{if } \left|\lambda_{V_k}\right| \leq F_{\max}/m_{C_i}, \quad k = x, y, z, \quad i = 1, 2, \ldots, n \\ u_k &= -\text{sign}\left(\lambda_{V_k}\right) F_{\max}/m_{C_i} \quad \text{if } \left|\lambda_{V_k}\right| > F_{\max}/m_{C_i}, \quad k = x, y, z, \quad i = 1, 2, \ldots, n \end{aligned} \tag{17}$$

Moreover, the time evolution of the co-state needed in Eq. 17 is described by

$$\dot{\boldsymbol{\Psi}} = -\begin{bmatrix} 0_{3\times 3} & I_{3\times 3} \\ A_1 & A_2 \end{bmatrix}^T \boldsymbol{\lambda} \tag{18}$$

where $\boldsymbol{\lambda}(t) \in \mathbb{R}^{6\times 1}, \forall \boldsymbol{\lambda}^T = [\boldsymbol{\lambda}_r, \boldsymbol{\lambda}_v]$. We consider each thrust component to be generated by an independent continuously operated engine. The optimal control problem is efficiently solved by iteratively searching for the values of the initial condition of the co-state vector $\boldsymbol{\lambda}(t_0)$ that minimizes the norm of the error between the desired and actual final states using the MATLAB® *fminsearch* routine. This error is found by propagating Eq. 1, with the control policy of Eq. 17. The initial time co-state vector guess for the first iteration is chosen to be equivalent to the unconstrained continuous control case such that

$$\boldsymbol{\lambda}(t_0) = -\Psi^{-1}(\Delta t)\left[\boldsymbol{\Phi}(\Delta t)\,\mathbf{x}(t_0) - \mathbf{x}\left(t_f\right)\right] \tag{19}$$

where $\Psi(t)$ is the convolution integral for the state vector due to the optimal unbounded control and $\boldsymbol{\Phi}(t)$ is the state transition matrix associated with the relative motion equations in Eq. 1.

4 Implementation of the two-phase hybrid controller

Having formulated the mathematical background for both phases of the proposed hybrid controller, namely the differential drag-based and optimal low-thrust portions, this section details the practical implementation of the algorithms. The block diagram of an integrated

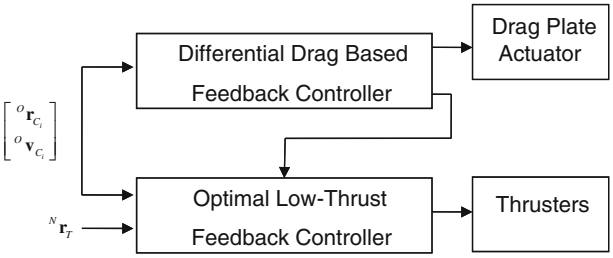

Fig. 4 Block diagram depiction of the two-phase hybrid controller

spacecraft control system with the hybrid controller is presented in Fig. 4. The inputs to the differential drag portion of the controller are the current position and velocity of the spacecraft in the Schweighart–Sedwick LVLH. Additionally, the maximum ballistic coefficient differential, the atmospheric density at the target's altitude at start time, and a tolerance on the final condition of stabilization are pre-computed prior to the start of the maneuver and made available as constants throughout the first phase of the maneuver. In particular, by maintaining a constant atmospheric density as a substitute for a varying real-world density in the control logic, a more satisfactory behavior is presented in the obtained trajectories. This can readily be seen by observing that the curves in the phase planes on which the differential drag-based portion of the hybrid controller is based (Fig. 1) must be kept constant. By continuously changing the atmospheric density, the controller's performance is significantly degraded as it seeks to continuously modify such curves.

During the first phase of the hybrid controller, the differential drag algorithm as presented in Sect. 2 is implemented on each chaser spacecraft with relaxation of the noted assumptions. At each time step, the differential drag algorithm determines a desired u_y for the given chaser spacecraft in the LVLH coordinate frame. This desired control is then translated to the corresponding rotation command for each set of drag plates as depicted in the three Cases in Fig. 2 such that the chaser cross-wind section area S_{C_i} affects the ballistic coefficient differential in Eq. 5. It is important to note that this is only a desired control and that the true effect of the change in S_{C_i} appears after interaction with the other parameters in Eqs. 4 and 5 as will be discussed in Sect. 5. Furthermore, in order to account for different ballistic coefficients between the chaser and target, the chaser's ballistic coefficient can be adjusted to match the target in the case when the commanded $u_y = 0$ by simple rotation of the panels. The required zero-state cross-wind section area for each chaser $S_{C_i 0}$ can be found by solving

$$S_{C_i 0} = \frac{C_{D_T} S_T m_i}{m_T C_{D_i}} \tag{20}$$

In particular, the following procedure is followed for implementing the differential drag portion of the hybrid controller in order to cope with nonlinear dynamics, biased atmospheric density, different ballistic coefficients and sensor noise:

1. From the generic chaser's initial conditions the feedback stabilizing algorithm is run until a nearly stable orbit around the target is reached. As the ideal case $z_1 = z_2 = 0$ can not be obtained under the effects of varying atmospheric density and sensor noise, this occurs when a predetermined tolerance on both parameters is obtained such that $z_1 \leq z_{1,\text{tol}}$ and $z_2 \leq z_{2,\text{tol}}$. The criteria to establish this tolerance is presented in Sect. 5.
2. The open loop analytical solution described in Sect. 2 is run until the distance between chaser and target starts increasing instead of decreasing.

Table 1 Simulation parameters

m_T (kg)	10
m_{C_1} (kg)	11
m_{C_2} (kg)	9
S_P (m^2)	0.25
S_T (m^2)	0.75
$S_{C_1,\min}$, $S_{C_2,\min}$ (m^2)	0.25
$S_{C_1,\max}$, $S_{C_2,\max}$ (m^2)	1.25
S_{C10} (m^2)	0.7857
S_{C20} (m^2)	0.7105
C_{D_T}	2.2
$C_{D_{C_1}}$	2.31
$C_{D_{C_2}}$	2.09
$\Delta BC_{C_1,\max}$ (m^2/kg)	0.0975
$\Delta BC_{C_2,\max}$ (m^2/kg)	0.1253
$\Delta BC_{C_1,\min}$ (m^2/kg)	−0.1125
$\Delta BC_{C_2,\min}$ (m^2/kg)	−0.107
$h(t_0)$ (km)	356
$F_{\max}$ (mN)	5
Δt_{opt} (s)	100

The rotation of the system of drag plates is not instantaneous in simulation in order to model the movement of drag plates on an actual spacecraft. The drag plates react to each new command by rotating between an open and a closed configuration (and vice versa) linearly, with ten seconds required to complete a full rotation. This implies the possibility of not full rotations in case the command is faster than 0.1 Hz.

Upon completion of the first phase of the hybrid controller, the drag plates on the chaser spacecraft are rotated to correspond to CASE 2 in Fig. 2 to make its cross-wind section area as near to that of the target spacecraft as possible and a flag is set to transfer translational control of the spacecraft to the optimal low-thrust portion of the controller. The inputs to this portion of the controller are again the position and velocity of the chaser spacecraft in the LVLH frame but also include the position of the target spacecraft in the inertial frame and a parameter to select the period of re-computation of the controls Δt_{opt} and a final rendezvous guess time t_f. This parameter provides the designer with a trade-space between computation speed and optimality.

5 Numerical simulations

This section reports the results of two sample numerical simulations. Two chaser spacecraft and the target, described in Table 1, are propagated from the initial conditions reported in Tables 2 and 3.

The first sample simulation employs the differential drag analytical approach described in Sect. 2, implemented as in Sect. 4. When the differential drag controller has completed its sequence, the thrusters take over, in order to reduce the residual error between the chaser

Table 2 Target spacecraft initial conditions

$a_T = 6713889.83$ m
$e_T = 0.01$
$i_T = 51.9412°$
$\Omega_T = 206.3577°$
$\omega_T = 101.0711°$
$\nu_T = 108.0848°$

Table 3 Chaser spacecraft initial positions in LVLH

$\mathbf{r}_{C_1}(t_0)$ (m)	[1000, 2000, 10]
$\mathbf{r}_{C_1}(t_0)$ (m)	[−1000, −2000, −10]
$\mathbf{v}_{C_2}(t_0)$ (m/s)	[−0.0084, −1.7018, −0.0063]
$\mathbf{v}_{C_2}(t_0)$ (m/s)	[0.0094, 1.7020, 0.0063]

spacecraft and the target spacecraft. This error is due to the assumptions made in Sect. 2 in order to develop the analytical controller. The following more realistic assumptions are considered for the simulations:

1. The atmospheric density is not constant. It is generated according to the exponential atmospheric model of Vallado (2004; p. 437, Table 8-4) . The exponential model follows the expression $\rho(h) = \rho_0 e^{\left(\frac{-(h-h_0)}{SH}\right)}$, where h is the altitude above the Earth's surface, and the parameters ρ_0, h_0, and SH are updated according to the altitude range, following a look-up table approach (Vallado 2004; p. 437, Table 8-4). For simulation purposes a bias is added to the generated density values, in order to realistically reproduce a limited knowledge of the atmospheric density. A constant error of +30% in the atmospheric density knowledge is here considered.
2. The gravity force is nonlinear (up to J_4).
3. The target's orbit is eccentric.
4. Disturbances are present (solar radiation pressure, third body effect).
5. Carrier-phase differential GPS (CDGPS) is supposed to be the sensor for relative navigation. The errors here considered are of the order of 5 cm for relative position and 1 cm/s for relative velocity. The chosen values follow state-of-the-art relative navigation techniques (Ferguson et al. 2001; Bordner and Wiesel 2006). This is implemented by adding white noise signals to LVLH position and velocity vectors. The white noises are such that the variance for the relative position is $\sigma_{\text{pos}} = (5/3)^2$ while the variance for the relative velocity is $\sigma_{\text{vel}} = (1/3)^2$. With these choices, 99% of the measurements are affected by a maximum error of 5 cm for relative position and 1 cm/s for relative velocity.

The second simulation uses only thrusters on the same time frame of simulation 1, in order to compare the fuel expenditure and show the amount of saving by using differential drag.

The tolerances in reaching the stable condition for the feedback stabilizing drag controller are found to be strongly dependent on the target spacecraft eccentricity. Numerical simulations show a satisfactory behavior when

$$z_{1,\text{tol}} = 10^2 e_T, \quad z_{2,\text{tol}} = 10^{-1} e_T \tag{21}$$

Table 4 Simulation Test Case 1 results: fuel consumption and starting points for the low-thrust phase

Chaser 1	Chaser 2
$I = 2.18$ mNs	$I = 19.4$ mNs
$\Delta V = 2 \times 10^{-4}$ m/s	$\Delta V = 2 \times 10^{-3}$ m/s
Thrusting start: $\mathbf{r}_{C_1}$ (m) = [−58.75, −148.45, 21.54]	Thrusting start: $\mathbf{r}_{C_2}$ (m) = [−47.83, −440.90, −7.75]
Total maneuver time: 10.83 h	Total maneuver time: 9.33 h

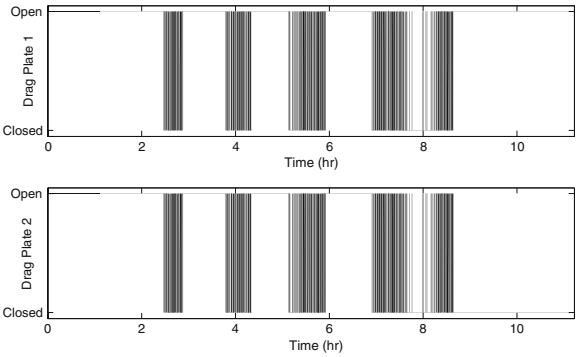

Fig. 5 Simulation Test Case 1: drag plates control sequence for Chaser 1. In this figure and in Fig. 6, the open configuration indicates that the chaser is configured as in Fig. 2, CASE 1; the closed configuration indicates that the chaser is configured as in Fig. 2, CASE 3; the remaining indicates CASE 2

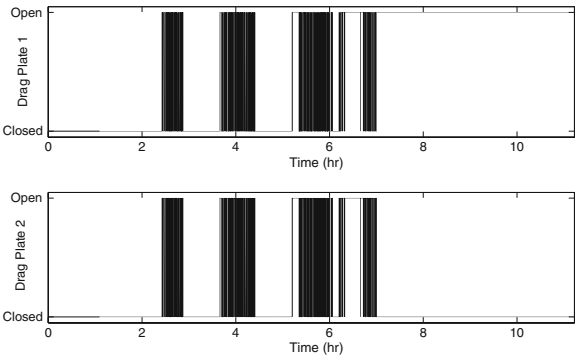

Fig. 6 Simulation Test Case 1: drag plates control sequence for Chaser 2.

5.1 Simulation Test Case 1: differential drag and optimal low thrust control

The main numerical results regarding the propelled phase for Simulation Test Case 1 are reported in Table 4. The time required for completing the maneuver is 10.8 hours and 9.3 hours for Chaser 1 and Chaser 2 respectively. The drag plates of the chasers start from the same configuration of the target, i.e. one of the two couples of plates is closed (see Fig. 2).

Figures 5 and 6 show the drag plates control history for chaser one and two. In particular, the drag plates are supposed to be opened and closed in couples, by rotating the plates which are symmetric with respect to the spacecraft in opposite directions, so that attitude effects can be compensated (see Fig. 2). It is worth noting that given a maneuver time frame of more than ten hours, the rotations of the plates depicted in Figs. 5 and 6 occur at feasible rates, according to the linear law described in Sect. 4.

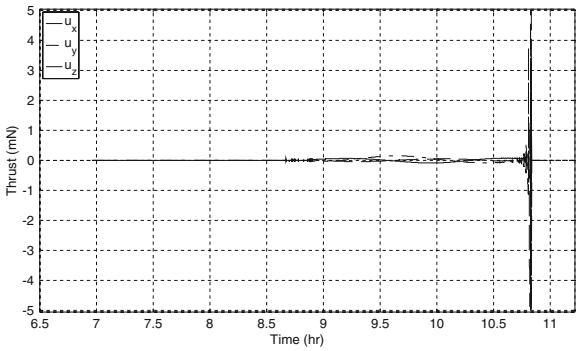

Fig. 7 Simulation Test Case 1: low-thrust control sequence for Chaser 1

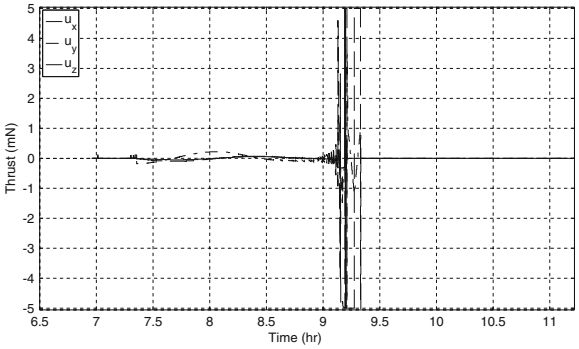

Fig. 8 Simulation Test Case 1: low-thrust control sequence for Chaser 2

Figures 7 and 8 depict the two chasers' thrust history, demonstrating active thruster control only near the end of the maneuver, after the drag controller has completed the feed-forward phase. Furthermore, Figs. 7 and 8 show that the thrust limitations are respected.

Figures 9 and 10 show the rendezvous trajectories of the two chasers in different views in the LVLH reference frame. The two chasers reach the target without any collision.

A further advantage of the proposed new drag plates' concept, already mentioned in the introduction of the paper, is that no coasting phases are required with respect to the work of Bevilacqua and Romano (2008), optimizing the overall maneuver required time.

In the paper by Bevilacqua and Romano (2008), the whole system of spacecraft, to include the target spacecraft, was maneuvered by changing each spacecraft's cross-wind section area. Two major disadvantages of this approach are that the target's orbit can decay more than might be desired and that a centralized control system is required whereby paddle control signals are sent throughout the system of chaser spacecraft and target spacecraft at each time step. In this work, we seek to overcome both of these disadvantages by assuming the target to not maneuver (which implies also that it is not increasing its drag and so its decay) and allowing each chaser to independently control its own cross-wind section area.

5.2 Simulation Test Case 2: optimal low thrust only

The main numerical results for Simulation Test Case 2 are reported in Table 5. The initial guess for the t_f in the fuel-optimal control algorithm is chosen to be the same as the total maneuver times given in Table 4.

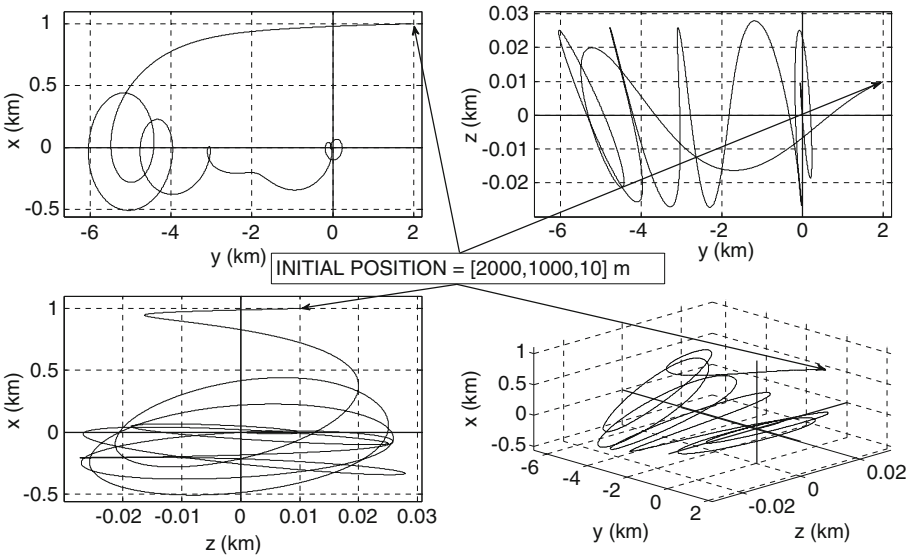

Fig. 9 Simulation Test Case 1: trajectory of Chaser 1

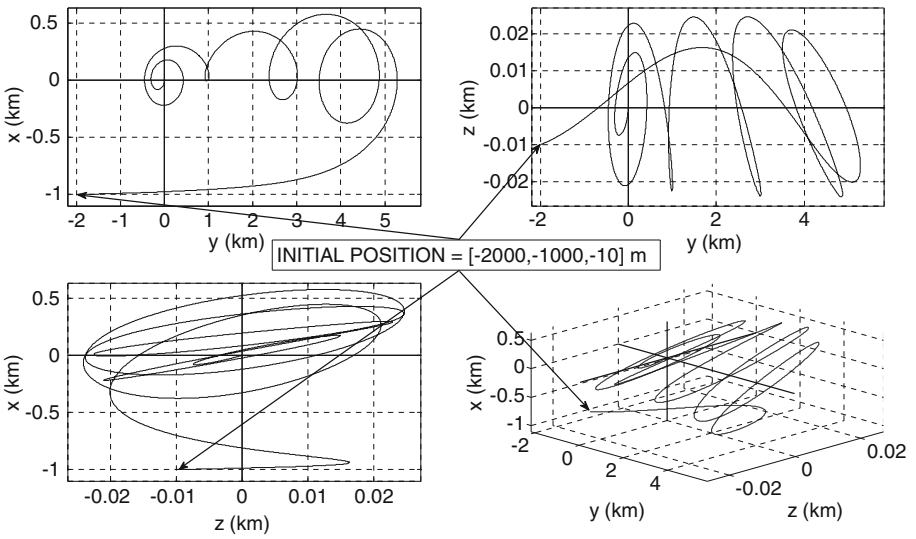

Fig. 10 Simulation Test Case 1: trajectory of Chaser 2

Table 5 Simulation Test Case 2 results: fuel consumption

Chaser 1	Chaser 2
$I = 40.5$ mNs	$I = 19.8$ mNs
$\Delta V = 3.68 \times 10^{-3}$ m/s	$\Delta V = 2.21 \times 10^{-2}$ m/s
Total maneuver time: 10.14 h	Total maneuver time: 8.68 h

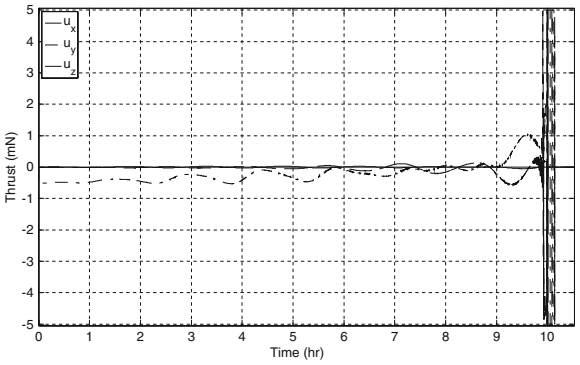

Fig. 11 Simulation Test Case 2: low-thrust control sequence for Chaser 1

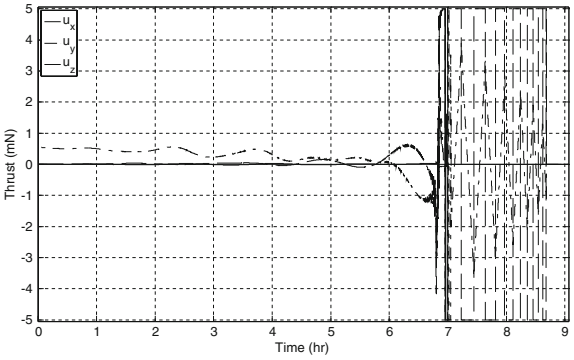

Fig. 12 Simulation Test Case 2: low-thrust control sequence for Chaser 2

Figures 11 and 12 are the chasers' thrust histories when the maneuver is performed using thrusters only. In this simulation the engines are used throughout the whole maneuver and the thrusters' capability is exploited more than in the previous simulation, still respecting the constraint on the maximum allowed thrust on each direction.

Figures 13 and 14 show the rendezvous trajectories of the two chasers in different views in the LVLH reference frame. Both the chasers reach the target state vector. As expected, comparison of Tables 4 and 5 yields a dramatic propellant savings for the combined differential drag and low-thrust controller against the low-thrust controller.

An additional advantage of the differential drag controller versus the optimal thrusting logic can be seen comparing the trajectories (Figs. 9 vs. 13 and 10 vs. 14). The trajectories generated by the differential drag controller remain more bounded than the ones obtained through optimal thrusting. This is due to the differential drag stabilizing algorithm that minimizes the harmonic oscillation amplitude while driving the secular part of the dynamics at zero (see Fig. 1), within the tolerance of Eq. 21.

5.3 Limitations on the usage of the differential drag logic for multi-spacecraft rendezvous scenarios

This section highlights the limitations on the usage of the proposed differential drag control algorithm. The main assumptions made in order to develop an analytical logic are constant atmospheric density and circular orbit. Numerical simulations have shown how these and other minor assumptions can be removed to allow the presented stabilizing and open-loop differential drag algorithms to be implemented to cope with uncertainties, sensors noises and,

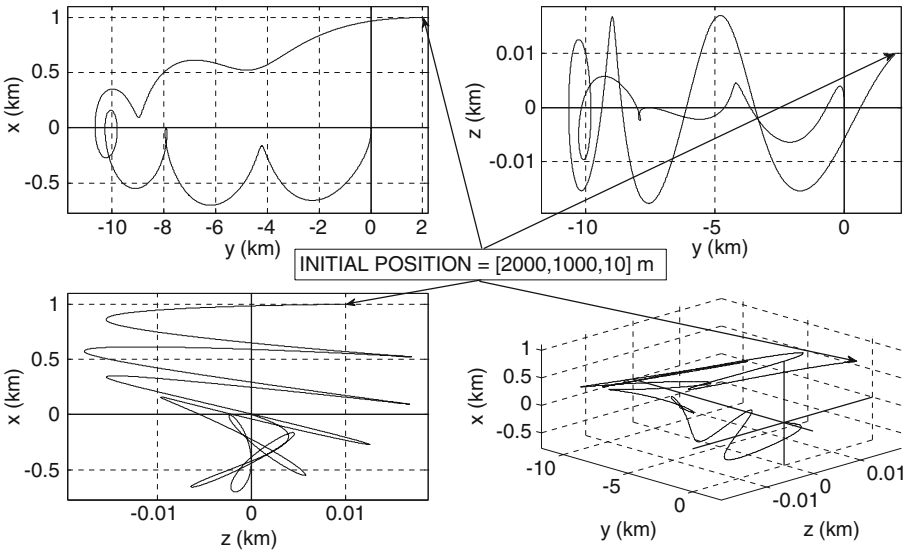

Fig. 13 Simulation Test Case 2: trajectory of Chaser 1

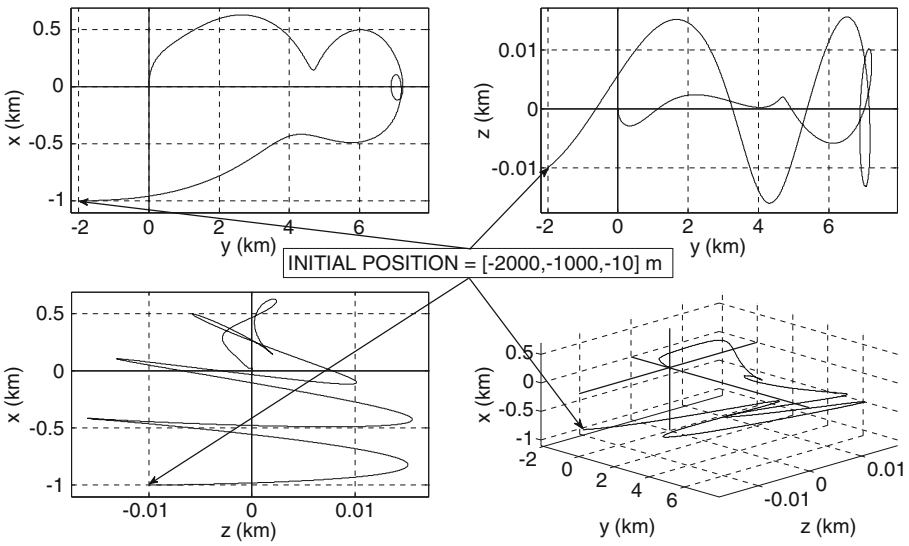

Fig. 14 Simulation Test Case 2: trajectory of Chaser 2

in particular, the non-modeled dynamics (e.g. eccentricity) and non-constant atmospheric density.

In particular, the presented numerical simulations assume a positive, constant 30% error on the knowledge of the density. An improved performance of the controller is obtained if the constant density value provided to the logic is lower than the typical values of the given altitude, while inputting a higher density value with respect to the typical ones degrades the performance until the system becomes fully uncontrollable. This can be justified in that by considering a lower atmospheric density, the actual control capability of each considered

chaser spacecraft is underestimated which still produces satisfactory results. However, by considering a higher atmospheric density than what is typical, the actual control capability of each chaser spacecraft is overestimated and the spacecraft tend to diverge rather than converge to the equilibrium solution. Therefore, this can be simply addressed by always under-estimating the atmospheric density expected at the typical altitudes of maneuvering. This can be done choosing an atmospheric density model, computing the target spacecraft's atmospheric density at the initial time, and subtracting at least 30% from the result to account for density model inaccuracies.

With regard to the eccentricity of the target's orbit, numerical simulations show that the differential drag-based portion of the controller can handle eccentric orbits. However, the disadvantage of using the hybrid controller for highly eccentric orbits is that the stable motion of the chaser spacecraft that is obtained after the stabilization phase maintains a high value for the amplitude of the residual harmonic motion. Thus, the differential drag portion of the controller cannot bring the chaser near to the target and the benefits of this algorithm become negligible. Numerical simulations show that a reasonable boundary on the eccentricity appears to be 0.02.

6 Conclusion

This work presents a hybrid technique which enables multiple-spacecraft rendezvous and rendezvous to a target spacecraft with low usage of propellant. The combination of differential drag from far away distances and low-thrust engines for the final approach to the target is the key factor of this research. In particular, the spacecraft are considered equipped with drag plates whose orientation can be changed with respect to the atmosphere wind direction, in order to control the amount of differential drag among them. In the final phase of the maneuver, a fuel-optimal continuous low-thrust controller drives the spacecraft to the target. Both the differential and fuel optimal controllers are based on linear dynamics, but are demonstrated here through numerical simulations to be feasible solutions for a high fidelity model of the orbital environment with its nonlinear effects, including solar, atmospheric, third body and up to J_4 gravitational effects.

Starting from a previous work by the authors, important developments are herein presented for the completely analytical differential drag approach. In particular, the implementation of drag plates is improved with respect to previous work by the authors, in order to allow the algorithm to be run independently on each chaser spacecraft and allow for reduced maneuvering times. Furthermore, new analytical breakthroughs are reported for the closed form solution control sequence based on differential drag.

Numerical simulations are included to confirm the advantage in terms of propellant consumption of using a hybrid approach with both differential drag and fuel-optimal low-thrust engines over only a fuel-optimal approach with low-thrust engines. In summary, the concept of variable drag plates on each of the chaser spacecraft appear to provide a feasible and low-risk ability to generate requisite drag differentials to effect orbit stabilization near a desired target spacecraft from which low-thrust control algorithms can be employed to effect precise rendezvous.

Acknowledgments This research was partially supported by DARPA. This research was performed while Dr. Bevilacqua was holding a National Research Council Research Associateship Award at the Spacecraft Robotics Laboratory of the US Naval Postgraduate School.

References

Bordner, R.E., Wiesel, W.E.: Trajectory estimation for satellites clusters. J. Guid. Control Dyn. **29**(1), 172–178 (2006).

Bevilacqua, R., Romano, M.: Optimal guidance of proximity maneuvers for a spacecraft with hybrid on-off continuous and impulsive thrust. AIAA J. Guid. Control Dyn. **30**(4), 1175–1178 (2007)

Bevilacqua, R., Romano, M.: Rendezvous Maneuvers of multiple spacecraft using differential drag under J2 perturbation. AIAA J. Guid. Control Dyn. **31**(6), 1595–1607 (2008)

Bevilacqua, R., Romano, M., Curti, F.: Decoupled-natural-dynamics model for the Relative Motion of two spacecraft without and with J2 perturbation. Accepted for publication, to appear on the Nonlinear Dyn. Syst. Theory (2009)

Campbell, M.E.: Planning Algorithm for Multiple Satellite Clusters. J. Guid. Control Dyn. **26**(5), 770–780 (2003)

Clohessy, W.H., Wiltshire, R.S.: Terminal guidance system for satellite rendezvous. J. Aerosp. Sci. **27**(9), 653–658 (1960)

De Ruiter, A., Lee, J., Ng, A.: A Fault-tolerant magnetic spin stabilizing controller for the JC2Sat-FF Mission. AIAA guidance, navigation and control conference and exhibit, Honolulu, Hawaii, 18–21 August 2008.

Ferguson, P., et al.: Formation flying experiments on the Orion. AIAA Space 2001—conference and exposition, Albuquerque, NM, 28–30 August 2001.

Guelman, M., Aleshin, M.: Optimal bounded low-thrust rendezvous with fixed terminal-approach direction. AIAA J. Guid. Control Dyn. **24**(2), 378–385 (2001)

Humi, M., Carter, T.: Fuel-optimal rendezvous in a central force field with linear drag. Paper AAS 01-236, pp. 1875–1892 (2001)

Kumar, B.S., Ng, A.: A bang-bang control approach to maneuver spacecraft in a formation with differential drag. AIAA Guidance, navigation and control conference and exhibit, Honolulu, Hawaii, 18–21 August 2008.

Kumar, K.D., Bang, H.C., Tahk, M.J.: Satellite formation flying using along-track thrust. Acta Astronaut. **61**, 553–564 (2007)

Leonard, C.L. Formation keeping of spacecraft via differential drag. M.Sc. Thesis, Massachusetts Institute of Technology, Cambridge, MA (1986)

Leonard, C.L., Hollister, W.M., Bergmann, E.V.: Orbital formation keeping with differential drag. AIAA J. Guid. Control Dyn. **12**(1), 108–113 (1989)

Palmerini, G.B., Sgubini S., Taini, G.: Spacecraft orbit control using air drag. Paper IAC-05-C1.6.10 (2005)

Pontryagin, L.S., Boltjanskiy, V.G., Gamkrelidze, R.V., Mishenko, E.F.: The Mathematical Theory of Optimal Processes. pp. 27–35. Willey-Interscience, New York, NY (1969)

Schweighart, S.A., Sedwick, R.J.: High-fidelity linearized J_2 model for satellite formation flight. AIAA J. Guid. Control Dyn. **25**(6), 1073–1080 (2002)

Starin, R.S., Yedavalli, R.K., Sparks, A.G.: Spacecraft formation flying maneuvers using linear-quadratic regulation with no radial axis input. AIAA Paper 2001-4029, AIAA guidance, navigation, and control conference and exhibit, Montreal, Canada (2001)

Vallado, D.A.: Fundamentals of Astrodynamics and Applications, 2nd edn. Microcosm Press, Hawthorne (2004)

Winetraub, Y., Tamir, R.: Using Differential Drag for Management of Nano-Satellite Constellations. http://netquire.com/insa/docs/UsingDifferentialDrag.pdf (2009).